Er-doped all-fiber laser mode-locked by graphitic carbon nitride nanosheets

Zikai Dong (董自凯)[1], Runqin Xu (徐润亲)[1], Wenhai Zhang (张文海)[2], Heyang Guoyu (郭于鹤洋)[1], Lingling Hua (华玲玲)[1], Jinrong Tian (田金荣)[1], and Yanrong Song (宋晏蓉)[1,*]

[1]*College of Applied Sciences, Beijing University of Technology, Beijing 100124, China*
[2]*Beijing Key Laboratory for Green Catalysis and Separation, College of Environmental and Energy Engineering, Beijing University of Technology, Beijing 100124, China*
**Corresponding author: yrsong@bjut.edu.cn*

Received February 15, 2018; accepted June 25, 2018; posted online July 30, 2018

Few-layer graphitic carbon nitride (g-C_3N_4) nanosheets were fabricated and utilized as a saturable absorber for mode-locking in an Er-doped fiber laser with net normal dispersion. The g-C_3N_4/polyvinyl alcohol (PVA) hybrid-film-based saturable absorber has a modulation depth of 4.01% and a saturation intensity of 7.5 MW/cm^2. By integrating g-C_3N_4-PVA mode-locker into the laser cavity, a mode-locked operation could be obtained. The achieved mode-locking pulse centered at 1530.3 nm has a pulse width of 530 ps. Its repetition rate is 40.8 MHz, and the corresponding signal-to-noise ratio is about 55 dB.

OCIS codes: 140.4050, 160.4236, 140.3500, 140.3510.
doi: 10.3788/COL201816.081402.

Two-dimensional (2D) materials (e.g., graphene, transition metal dichalcogenides, black phosphorus) demonstrate intriguing optical properties owing to their strong light–material interaction, high nonlinearity, and fast and broadband optical response[1–3]. Simultaneously, passively mode-locking technologies in fiber lasers, which include nonlinear polarization rotation (NPR), a nonlinear optical loop mirror (NOLM), and a semiconductor saturable absorber mirror (SESAM), have been widely investigated for their advantages in specific applications[4–6]. However, a series of problems, such as polarization instability of NPR, lower power magnitude of NOLM, and bandwidth limitations of SESAM, cannot be neglected. In recent years, graphene and some other 2D-materials-based saturable absorbers (SAs) show superior performance for generating ultrashort pulses in a variety of lasers[7–11]. Li *et al.* reported the low phase mode-locked fiber laser based on a single wall carbon nanotube (SWNT) and graphene oxide (GO)[12]. Wu *et al.* summarized the mode-locked and *Q*-switched laser performance (e.g., operating wavelength, optical bandwidth, repetition rate, and pulse energy) based on the 2D materials[13].

Driven by the excellent performances, it is intriguing to seek novel 2D materials as SAs. Very recently, several kinds of novel 2D materials have been successfully drawn into the passively mode-locked fiber lasers as SAs. One of them is perovskite nanocrystal. In 2016, an SA made of cesium lead halide perovskite nanocrystals ($CsPbX_3$, $X = Cl$, Br, I) was used in a passively mode-locked ytterbium-doped (Yb-doped) fiber laser[14]. In 2017, based on hybrid organic-inorganic perovskite ($CH_3NH_3PbI_3$) nanosheets at the wavelength of 1 μm, the *Q*-switched[15] and mode-locked[16] fiber lasers were, respectively, achieved. Another novel 2D material is graphitic carbon nitride (g-C_3N_4). In 2016, nonlinear optical effects of 2D-like C–N polymer nanosheets were investigated, and the 2D-like CN polymer was firstly used as an SA in an all-normal dispersion Yb-doped mode-locked fiber laser at 1.06 μm[17]. In 2017, SAs based on g-C_3N_4 nanosheets attracted more attention, with which a *Q*-switched Nd:$LuLiF_4$ solid laser, a *Q*-switched Er:Lu_2O_3 solid laser, and a *Q*-switched Ho,Pr:LLF solid laser were demonstrated at 1.3, 2.84, and 2.95 μm, respectively[18–20]. For convenience of comparison, Table 1 gives a summary of pulsed lasers using g-C_3N_4 as SAs for optical modulators. The results illustrate that the g-C_3N_4 is a broadband optical SA, and the g-C_3N_4 SA modulation depth can vary from 3.3% to 13.6%.

In this Letter, few-layer g-C_3N_4 nanosheets were fabricated. When mixing it with polyvinyl alcohol (PVA), a homemade g-C_3N_4/PVA film SA was acquired. Using it, an Er-doped mode-locked all-fiber laser was reached. The pulse-width is 530 ps at the wavelength of 1530.3 nm, and the repetition rate is 40.8 MHz. The signal-to-noise ratio is 55 dB, which means that the laser is stable. To the best of our knowledge, this is the first time an Er-doped mode-locked fiber laser based on g-C_3N_4 nanosheets is demonstrated.

The g-C_3N_4 powder was synthesized by thermal condensation of melamine[21]. 10 g of melamine powder (99%, Aldrich) was tempered at 550°C in an alumina crucible under an N_2 atmosphere for 4 h. After cooling down, 5.0 mg of light yellow bulk g-C_3N_4 powder was collected, which is shown in Fig. 1(a). The g-C_3N_4 nanosheets were acquired by the liquid exfoliation method. Then, the 5.0 mg g-C_3N_4 powder was added into distilled water and ultrasonicated pulverization for 9 h. After 3 h of standing at the room temperature, the undissolved powder g-C_3N_4 was removed, and then centrifuged for 15 min

Table 1. Different Pulsed Lasers Modulated by a g-C_3N_4 SA

Modulation Depth (%)	Wavelength (nm)	Pulse Width/Energy (ps/μJ)	Modulation Type	References
12.5	1066	310 ps	Mode-locking	[14]
3.3	2840	11.1 μJ	*Q*-switching	[16]
11.1/13.6	1320	6.2 μJ	*Q*-switching	[18]
4.1	1530	530 ps	Mode-locking	This work

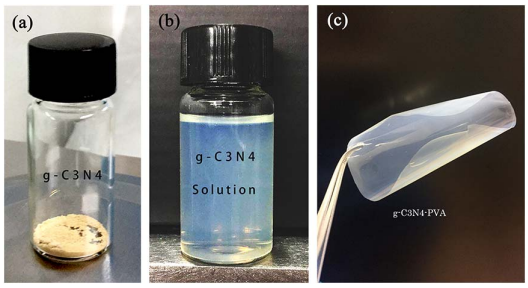

Fig. 1. Photographs of (a) the synthesized g-C_3N_4 powder, (b) 0.1 mg/mL g-C_3N_4 solution, and (c) the final g-C_3N_4/PVA hybrid film.

at 8000 r/min. The collected supernatant is exhibited in Fig. 1(b). The concentration of g-C_3N_4 was 0.1 mg/mL (measured by the weighing method). The g-C_3N_4/PVA was fabricated by the vertical evaporation method. The 8 mL g-C_3N_4 solution and 1.5 mg liquid phase PVA were mixed and stirred in the magnetic stirrer for 3 h. After that, the hybrid g-C_3N_4/PVA solution was dropped on the quartz plate and evaporated at room temperature. The final g-C_3N_4/PVA hybrid film was finished as illustrated in Fig. 1(c).

The crystal structure of g-C_3N_4 powder was investigated by an X-ray diffraction (XRD) instrument (BRUKER, D8 advance). The microstructure and thickness of g-C_3N_4 nanosheets were characterized by transmission electron microscopy (TEM) (JEOL, JEM-2100F) and atomic force microscopy (AFM) (WiTec, Alpha 300S), respectively. The morphology of the g-C_3N_4/PVA hybrid film cross section was measured by scanning electron microscopy (SEM) (Hitachi, SU-8020).

The XRD pattern displays a weak diffraction peak at 13.2° and a strong diffraction peak at 28°, as shown in Fig. 2(a). The two diffraction peaks can be defined as (100) and (002) planes, which represent the in-plane structural motif and the interplanar graphitic-like stacking of conjugated aromatic C–N segment, respectively[22]. The TEM and AFM photographs are exhibited in Figs. 2(b) and 2(c). These two images indicate that g-C_3N_4 flakes have a layered microstructure and nano-cluster structures. The nanocluster thickness is about 6.5 nm, calculating an interplanar stacking distance of n aromatic units of 0.326 nm (radiation: $\lambda = 0.15418$ nm, $2\theta = 28°$). The cluster structure may issue from a rolled structure, bulk material, and a

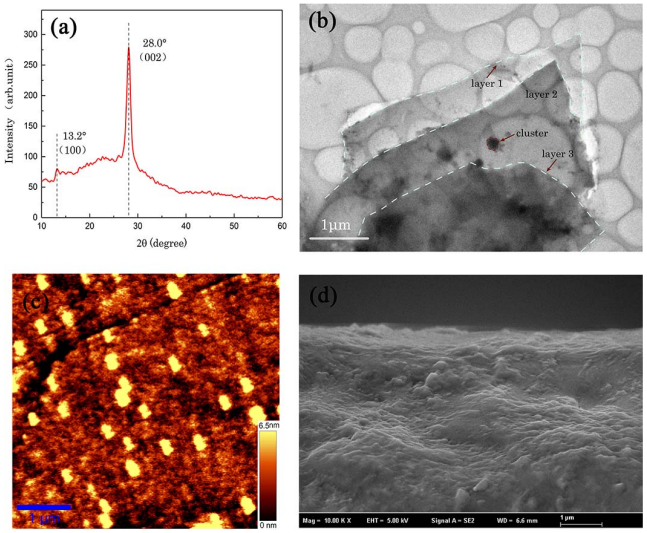

Fig. 2. (a) XRD pattern of g-C_3N_4 powder, (b) TEM photograph of g-C_3N_4 nanosheets, (c) AFM image of g-C_3N_4 nanosheets, (d) SEM image of the cross section of the g-C_3N_4/PVA hybrid film.

multilayered structure, which may affect the layered structure. The SEM image demonstrates the cross section of g-C_3N_4/PVA hybrid film, as illustrated in Fig. 2(d).

The nonlinear optical properties of the SAs based on g-C_3N_4/PVA hybrid film were performed by a Z-scan setup[23] equipped with a self-constructed femtosecond fiber laser (laser parameters: repetition rate is 73 MHz, pulse duration is 281 fs, center wavelength at 1035 nm). The result is shown in Fig. 3. The saturable absorption can be analyzed[24]: $T(I) = 1 - \alpha_0 \times \exp(-I/I_{\text{sat}}) - \alpha_{\text{ns}}$, where $T(I)$ is the transmission, α_0 is the modulation depth, α_{ns} is the nonsaturable absorbance, I is the incident intensity, and I_{sat} is the saturable intensity. By fitting the experimental data, the SA parameters α_0, α_{ns}, and I_{sat} are estimated to be 4.1%, 14.4%, and 7.5 MW/cm^2, respectively. It should be noted that the theoretical bandgap of g-C_3N_4 is ~2.67 eV, which corresponds to the longest absorption edge of ~465 nm. However, the saturable absorption response wavelength of g-C_3N_4 in the near-IR has also been experimentally demonstrated through some effective methods of narrowing the bandgap. These methods include heteroatom doping, defect control, multilayer structure, and heterojunction construction. Based on these facts, the operation of the g-C_3N_4 SA at 1.5 μm is mainly caused

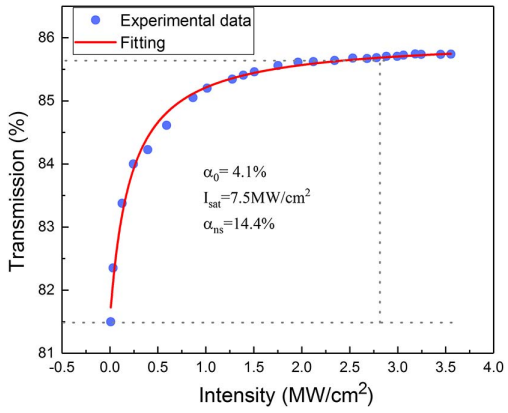

Fig. 3. Nonlinear transmission of the g-C_3N_4/PVA-SA.

by the joint action of the layered structure and nanocluster structure.

Figure 4 is the schematic of the passively mode-locked Er-doped fiber laser based on g-C_3N_4/PVA-SA. The laser is in a ring configuration, using Er-doped fiber (Liekki, Er110-4/125, 30 cm) as the gain medium. A 980 nm laser diode was used as the pump source through a wavelength division multiplexer (WDM, 980/1550 nm). The laser operation direction was ensured by a polarization-dependent isolator (ISO, 1550 nm). The cavity polarization state and intra-cavity birefringence was regulated by the three-ring structure polarization controller (PC). The output power was controlled by the 10% intensity fiber coupler. The SA based on g-C_3N_4/PVA hybrid film was assembled by the sandwiching structure between two fiber ferrules.

These fiber devices were connected by two different types of fiber: one is an SMF-28, which has a dispersion value of 15 ps $\cdot$ (nm $\cdot$ km)$^{-1}$ at 1550 nm; and the other is OFS 980, which has a dispersion value of 13 ps $\cdot$ (nm $\cdot$ km)$^{-1}$. The net dispersion value is estimated as 0.055 ps^2, which ensures that the laser operates in the net normal dispersion regime and prohibits the traditional soliton forming in

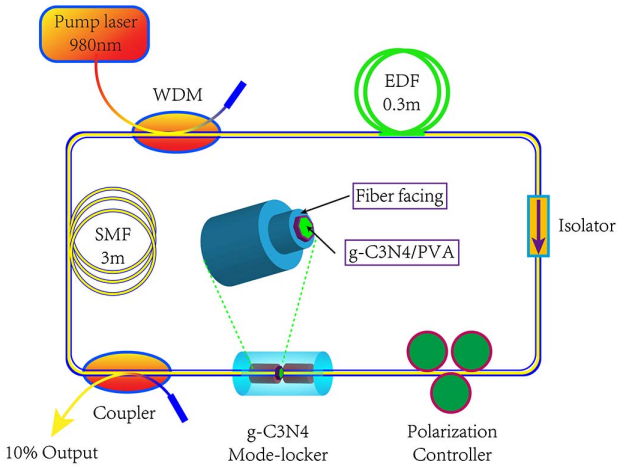

Fig. 4. Experimental setup of Er-doped mode-locked fiber laser with the g-C_3N_4/PVA SA using the sandwich structure.

the laser cavity. The total cavity length is about 5 m. When the fiber is long, the optical fiber birefringence effect is non-negligible, so in order to seek the effect of the g-C_3N_4/PVA-SA for establishing the mode-locking, the short length cavity is more suitable.

Before inserting the g-C_3N_4/PVA SA into the laser cavity, the continuous wave was always observed even when we adjusted the PC, and the mode-locked operation state cannot be established even when we varied the pump power and adjusted the PC state at every specific pump power (from zero to the maximum of 500 mW).

Once we inserted the g-C_3N_4/PVA SA into the laser cavity and adjusted the PC, the mode-locking operation state started. The condition of the operation state transition is the incident pump power up to the mode-locked threshold power (~80 mW) and the specific state of the PC. The performance of the stable mode-locked pulse laser was obtained from the g-C_3N_4/PVA SA, as demonstrated in Fig. 5. The output time-domain profile characteristics were monitored by a 4 GHz sampling oscilloscope (Tektronix, DPO 70604C) integrated with a high-speed 1.5 GHz photodetector (Newport, 818-BB-35F). The frequency-domain properties were tested using an optical spectrum analyzer (Yokogawa, AQ6370C); the radio frequency (RF) spectrum was analyzed with a spectrum analyzer (Agilent, E4447A). The power was measured by the laser power meter (gentec-eo, UNO).

The typical mode-locking optical spectrum is shown in Fig. 5(c). The 3 dB bandwidth is about 0.2 nm at the center wavelength of 1530 nm. Figure 5(a) displays the mode-locking pulse train. Separation between adjacent pulses is about 25.9 ns, which matches well with the cavity length of 5.02 m. The mode-locked laser pulse has a full width at half-maximum (FWHM) of 530 ps, as inserted in Fig. 5(a), indicating that the optical pulse is chirped (Gauss pulse assumption, the expected time

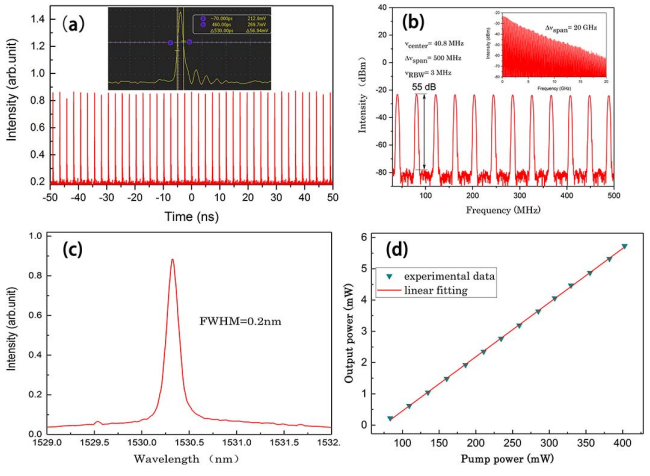

Fig. 5. Characteristics of the mode-locked fiber laser using a g-C_3N_4/PVA SA. (a) Output pulse train, time-domain pulse profile inserted. (b) RF output spectrum, RF spectrum in 20 GHz span inserted. (c) Typical optical spectrum. (d) Output power varies with the pump power.

bandwidth product for the transform-limited Gauss pulse is 0.441, the 0.2 nm bandwidth corresponding transform-limited pulse width is about 60 ps). The mode-locked pulse formed in the dissipative system is not the same as the traditional soliton formation, in which the g-C_3N_4/PVA SA plays a key role. The RF spectrum was measured and depicted in Fig. 5(b), and the signal-to-noise ratio is over 55 dB in a wide band from 0 to 500 MHz. The inserted figure in Fig. 5(b) is the 20 GHz range RF spectrum. The long range RF spectrum indicates that no *Q*-switched instability occurred, and the mode-locking operation state was stable. The relation between the incident power and output power was shown in Fig. 5(d). The output power increases linearly from 0.2 to 5.73 mW, corresponding to the pump power from 80 to 400 mW, where the slope efficiency is 1.4%.

In conclusion, we firstly introduced the SA based on g-C_3N_4 nanosheets into the 1.5 μm regime mode-locked fiber laser. Few-layer g-C_3N_4 nanosheets were fabricated, and a stable mode-locking operation was demonstrated based on the homemade g-C_3N_4/PVA SA. The pulse width of the mode-locking pulses is about 530 ps at 1530.3 nm. The repetition rate is 40.8 MHz, and the corresponding signal-to-noise ratio is about 55 dB. These SAs based on g-C_3N_4 nanosheets have advantages of easy fabrication, broadband optical response, and flexible thickness manipulation. This indicates that the g-C_3N_4 nanosheets can be a new candidate for passively mode-locked lasers.

This work was supported by the National Natural Science Foundation of China (No. 61575011), the Key Project of the National Natural Science Foundation of China (No. 61235010), and the Promotion Project of Beijing Municipal Institutions and Science and Technology Foundation (No. ykj-2017-00217).

References

1. S. L. Yu, X. Q. Wu, Y. P. Wang, X. Guo, and L. M. Tong, Adv. Mater. **29**, 1606128 (2017).
2. X. F. Liu, Q. B. Guo, and J. R. Qiu, Adv. Mater. **29**, 1605886 (2017).
3. Z. P. Sun, A. Martinez, and F. Wang, Nat. Photon. **10**, 227 (2016).
4. A. P. Luo, Z. C. Luo, H. Liu, X. W. Zheng, Q. Y. Ning, N. Zhao, W. C. Chen, and W. C. Xu, Opt. Express **23**, 10421 (2015).
5. X. L. Li, S. M. Zhang, H. Y. Han, M. M. Han, H. X. Zhang, L. M. Zhao, F. Wen, and Z. J. Yang, Opt. Express **23**, 10747 (2015).
6. F. Zou, Z. K. Wang, Z. W. Wang, Y. Bai, Q. R. Li, and J. Zhou, Opt. Laser Technol. **92**, 133 (2017).
7. W. J. Liu, L. H. Pang, H. N. Han, K. Bi, M. Lei, and Z. Y. Wei, Nanoscale **9**, 5806 (2017).
8. J. L. Zheng, Z. H. Yang, Z. M. Zhang, D. Y. Fan, and H. Zhang, ACS Photon. **4**, 1466 (2017).
9. Z. P. Sun, T. Hasan, F. Torrisi, D. Popa, G. Privitera, F. Q. Wang, F. Bonaccorso, D. M. Basko, and A. C. Ferrari, ACS Nano **4**, 8 (2010).
10. M. L. Liu, P. G. Yan, S. B. Fang, H. Teng, and Z. Y. Wei, Chin. Opt. Lett. **16**, 020007 (2018).
11. B. Guo, Chin. Opt. Lett. **16**, 020004 (2018).
12. X. H. Li, K. Wu, Z. P. Sun, B. Meng, Y. G. Wang, T. S. Wang, X. C. Yu, Y. Zhang, P. P. Shum, and Q. J. Wang, Sci. Rep. **6**, 25266 (2016).
13. K. Wu, B. H. Chen, X. Y. Zhang, S. F. Zhang, C. S. Guo, C. Li, P. S. Xiao, J. Wang, L. J. Zhou, W. W. Zou, and J. P. Chen, Opt. Commun. **406**, 214 (2018).
14. Y. Zhou, Z. P. Hu, Y. Li, J. Q. Xu, X. S. Tang, and Y. L. Tang, Appl. Phys. Lett. **108**, 261108 (2016).
15. P. F. Li, Y. Chen, T. S. Yang, Z. Y. Wang, H. Lin, Y. H. Xu, L. Li, H. R. Mu, B. N. Shivananju, Y. P. Zhang, Q. L. Zhang, A. L. Pan, S. J. Li, D. Y. Tang, B. H. Jia, H. Zhang, and Q. L. Bao, ACS Appl. Mater. Int. **9**, 12759 (2017).
16. B. Huang, J. Yi, G. B. Jiang, L. L. Miao, W. Hu, C. J. Zhao, and S. C. Wen, Opt. Mater. Express **7**, 1220 (2017).
17. Y. Zhou, M. Zhao, S. W. Wang, C. X. Hu, Y. Wang, S. Yan, Y. Li, J. Q. Xu, Y. L. Tang, L. F. Gao, Q. Wang, and H. L. Zhang, Opt. Lett. **41**, 1221 (2016).
18. M. Q. Fan, T. Li, G. Q. Li, H. Y. Ma, S. Z. Zhao, K. J. Yang, and C. Krankel, Opt. Lett. **42**, 286 (2017).
19. M. Q. Fan, T. Li, G. Q. Li, S. Z. Zhao, K. J. Yang, S. Y. Zhang, B. T. Zhang, J. Q. Xu, and C. Krankel, Opt. Express **25**, 12796 (2017).
20. X. C. Gao, S. X. Li, T. Li, G. Q. Li, and H. Y. Ma, Photon. Res. **5**, 33 (2017).
21. S. C. Yan, Z. S. Li, and Z. G. Zou, Langmuir **25**, 10397 (2009).
22. Q. Huang, J. Yu, S. Cao, C. Cui, and B. Cheng, Appl. Surf. Sci. **358**, 350 (2015).
23. K. X. Li, Y. R. Song, Z. H. Yu, R. Q. Xu, and J. R. Tian, Laser Phys. Lett. **12**, 105103 (2015).
24. E. Garmire, IEEE J. Sel. Top. Quantum Electron. **6**, 1094 (2000).